

Soliton Systems at Finite Temperatures and Finite Densities

Oliver Schwindt and Niels R. Walet
Dept. of Physics, UMIST, Manchester M60 1QD, UK
(Dated: November 20, 2018)

The finite-density and finite-temperature phase portraits of the baby-Skyrme and Skyrme models are investigated. Both grand-canonical and canonical approaches are employed. The grand-canonical approach can be used to find the “natural” crystal structure of the baby-Skyrme model and it is shown to have triangular symmetry. The phase portraits include solid, liquid and phase-coexistence between solids and vacuum states. Furthermore, a chiral phase transition can be observed for both models. The phase portrait of the Skyrme model is compared with that expected of strongly interacting matter, and we also contrast our results to other models.

PACS numbers: 12.39.Dc, 21.65.+f, 05.10.-a, 73.43.-f

I. INTRODUCTION

One of the great questions in the theory of strong interactions is the behavior of baryonic matter at finite density and finite temperatures. Even though it is widely believed that quantum chromo-dynamics (QCD) is the correct theory to describe the strong interactions, its non-perturbative nature makes it extremely difficult to describe the low energy consequences of the theory. Lattice QCD [1] is the preferred numerical technique to study the QCD Lagrangian directly. Here, QCD is modeled non-perturbatively by discretising the theory on a lattice, and a numerical approximation is made to the path integral describing either the Euclidean time evolution or the thermodynamics of the theory. The masses of mesons, baryons, and glueballs have already been calculated to reasonable accuracy [2]. The limitations of the approach are both numerical (momentum cut-off, finite lattice size), and more theoretical. The most important difficulty is the description of fermions on the lattice. Since lattice QCD relies on using Monte Carlo methods, computing power is another of the key limitations. If sufficient powerful computers were available, the inaccuracies due to discretising QCD could be reduced by adopting larger gridsizes. Therefore, as computing power increases in future, more accurate results will be achieved. Even then, dealing with a finite density of fermions is an especially tricky problem, since the fermionic determinant to be calculated becomes complex, leading to various instabilities.

Due to these difficulties, it is quite common to use models to study the phase diagram of strongly interacting matter. Recent examples of such approaches can for instance be found in studies by Rajagopal *et al* [3, 4], who describe the phase diagram using a Nambu-Jona-Lasino model [5] and a random matrix model [6]. The QCD phase diagram, obtained from a model with two massless quarks in Ref. [3]. A typical phase diagram shows a hadronic-matter phase, the quark-gluon plasma, and a color superconducting phase. Earth’s surface, in general, has a low temperature (0.025 eV) and a chemical potential much less than 1 GeV, and therefore we live in a (liquid) hadronic-matter phase. The most striking feature

of the phase diagram is the presence of a critical point. This separates an area where a first-order phase transition occurs, from one where a continuous path can be taken from the hadronic phase to the quark-gluon plasma phase. At the critical point itself, it is believed that there is a second-order phase transition. The position of the critical point is extremely difficult to model and has been estimated to have a temperature $T_E \approx 140 - 190$ MeV and a chemical potential of $\mu_E \approx 200 - 800$ MeV [3, 7]. The color superconducting phase cannot be modeled by the Skyrme model because color-flavor locking is observed, and in order to model it, three colors need to be considered rather than the $N_c = \infty$ approximation underlying the Skyrme model, which will be discussed later. The color superconducting phase will therefore not be discussed further.

The Skyrme model has a venerable history [8] in the non-perturbative description of nucleon structure and the low-energy behavior of baryonic matter, since it contains a good description of the long-wave length behavior of the dynamics of hadrons. As has been argued by ’t Hooft and Witten [9, 10, 11], this is closely related to the large-number-of-colors limit of QCD, in which baryons must emerge as solitons, in much the same way as happens in the Skyrme model. Alternatively, we can interpret the model in terms of chiral perturbation theory, in terms what is much like a gradient expansion in terms of the pion field. The model can be used to describe, with due care [12, 13], systems of a few nucleons, and has also been applied to nuclear and quark matter. Within the standard zero-temperature Skyrme model description there are signatures of chiral symmetry restoration at finite density, but in a rather special way, where a crystal of nucleons turns into a crystal of half nucleons at finite density, which is chirally symmetric only on average [14]. The question of the finite-temperature has never been addressed and would be of some interest. We shall also look at the two-dimensional Skyrme model, which has the advantage of being easier to interpret, but also has physical relevance; a special form of the two-dimensional Skyrme model has recently been developed for use in quantum Hall systems [15]. This model is obtained as an effective theory when the excitations relative to the $\nu = 1$ ferro-

magnetic quantum Hall state are described in terms of (a gradient expansion in) the spin density, a field with properties analogous to the pion field in nuclear physics [16]. Apart from obvious changes due to the number of dimensions, the new approach differs from the historical Skyrme model by having a different time-dependent term in the Lagrangian, and the appearance of a non-local interaction, where the topological charge density at different points interacts through the Coulomb force. In the limit of large Skyrmions this last term can be approximated by a more traditional local “Skyrme term”, which is quartic in the fields, leading to the standard baby-Skyrme model with local interactions. Even with the non-local complication the model is on the whole remarkably similar to the nuclear Skyrme model. The Skyrme-field effective degrees of freedom describe the ground state of such systems, and probably also the low energy dynamics and thermodynamics, so that we can ask similar questions about the finite-density physics as for baryonic matter.

In this paper we shall consider the local baby Skyrme model, which can be regarded as the 2D version of the traditional 3D nuclear one. We can also extrapolate to one dimension. The model obtained in that way is the sine Gordon model expressed in terms of an unit complex field. All of these models contain a topologically conserved charge, which in the three-dimensional case is identified with baryon number. This gives rise to topological solitons, which in nuclear physics are identified as baryons. Since the behavior of nuclear matter at high densities is expected to reveal, probably by one or two phase transitions, the substructure of baryonic matter, it is interesting to study this phenomenon in Skyrme models. At the same time it allows us to look at the phase diagram of quantum Hall Skyrmionic systems, which may well be the easiest way to calculate parts of the phase diagram of the underlying electronic model.

At finite density but zero temperature the Skyrme models and the sine Gordon model have a crystalline structure, which consist of regularly spaced solitons. In the one-dimensional case, where exact solutions exist [17], this is known to be a zero temperature artifact, and we have a liquid at any finite temperature, no matter how small. In the nuclear Skyrme model we would like to find a fluid, to mimic the quantum liquid behavior expected in nuclear matter [18]. In order to appreciate the subtleties involved, one must understand that the Skyrme model, as a classical field theory, can be understood as a semi-classical (large action) limit of a quantum theory. Clearly the quantum fluctuations in the underlying theory could be large enough to wash out the crystalline structure, as happens for the sine Gordon model. In the special case of one space dimension it is also well known that thermal and quantum fluctuations play exactly the same role, and thermal fluctuations also break the crystalline state. For the Skyrme and baby Skyrme models it is not easy to access the quantum fluctuations, since the field theories are non-renormalisable, but we can access the thermal fluc-

tuations (with care, because nonrenormalisability plays a role in the thermodynamics as well!). Furthermore, we might well wish to study the physics of these systems at temperatures where thermal fluctuations dominate the physics. Therefore, we shall concentrate on the finite temperature phases of these classical field theories.

The most direct approach to the problem is to perform a Monte-Carlo (Metropolis algorithm based) study of the partition function of each of these models. As we shall argue below the least obvious aspect in such an approach is how to deal with the topological conservation laws. Rather than immediately tackle the 3D model, we shall first concentrate on the (local) 2D model. This has the advantage that the visualization of, and also the understanding gained by, the results is much more straightforward. The extensions to quantum-Hall Skyrmions are under way and will be presented elsewhere [19]. We expect the current for the QHE solitons to be very similar to the results reported here.

This paper is organized as follows. In Sec. II we discuss the formalism succinctly. In the next section, Sec. III we discuss in detail the results obtained in our simulations (a small excerpt has already been published in Refs. [20, 21]). We draw some conclusions, and give an outlook for possible future work in Sec. IV.

II. FORMALISM

A. Lagrange density

The Lagrange density for Skyrme models can be given as [8, 22]

$$\mathcal{L} = \frac{1}{2}(\partial_\mu \phi_k)^2 - \frac{1}{4}(\partial_\mu \phi_k \partial^\mu \phi_k \partial_\nu \phi_l \partial^\nu \phi_l) + \frac{1}{4}(\partial_\mu \phi_k \partial^\mu \phi_l \partial_\nu \phi_k \partial^\nu \phi_l) + \frac{m_\pi^2}{f_\pi^2 e^2}(\phi_0 - 1), \quad (1)$$

which as long as we take the space index $\mu = 0, 1, \dots, d$ to describe $d+1$ dimensional space, and the field components $k, l = 1, \dots, d+1$ to describe a $d+1$ dimensional unit vector, can describe the Sine-Gordon theory ($d=1$), the baby Skyrme model ($d=2$) and the nuclear Skyrme model ($d=3$). The Lagrange density can be separated into a kinetic and a potential term

$$\mathcal{L} = \mathcal{T}[\phi] - \mathcal{V}[\phi], \quad (2)$$

where

$$\mathcal{T}[\phi] = \frac{1}{2} \partial_t \phi_a \partial_t \phi_b \mathcal{M}_{ab}[\phi], \quad (3)$$

$$\mathcal{M}_{ab}[\phi] = \delta_{ab} + \partial_i \phi_c \partial_i \phi_c \delta_{ab} - \partial_i \phi_a \partial_i \phi_b, \quad (4)$$

$$\mathcal{V}[\phi] = \frac{1}{2} \partial_i \phi_a \partial_i \phi_a + \frac{m_\pi^2}{f_\pi^2 e^2} (1 - \phi_0) + \frac{1}{4} ([\partial_i \phi_a \partial_i \phi_a]^2 - [\partial_i \phi_a \partial_j \phi_a][\partial_i \phi_b \partial_j \phi_b]) \quad (5)$$

For our later calculation we need we need the expression for the energy density, $\mathcal{T} + \mathcal{V}$, which for the Skyrme model becomes

$$\mathcal{E} = \frac{1}{2} \partial_t \phi_a \partial_t \phi_b \mathcal{M}_{ab}(\phi(\mathbf{x})) + \mathcal{V}(\phi(\mathbf{x})) . \quad (6)$$

The two sets of constraints (implemented by the delta-functions in the integrals) are $\phi^2 - 1 = 0$ and $\dot{\phi} \cdot \phi = 0$ at each point in space, where the first constraint forces ϕ to have unit length and the second constraint follows by taking the time derivative of the first constraint.

In 3D the topological charge density, which was identified by Skyrme with the baryon-number density operator, is given by

$$\begin{aligned} \mathcal{B}(\mathbf{x}) &= \frac{1}{12\pi^2} \varepsilon^{0\sigma\rho\nu} \varepsilon^{\alpha\beta\gamma\delta} \phi_\alpha \partial_\nu \phi_\beta \partial_\sigma \phi_\gamma \partial_\rho \phi_\delta \\ &= \frac{1}{2\pi^2} \det(\phi, \partial_x \phi, \partial_y \phi, \partial_z \phi) , \end{aligned} \quad (7)$$

with simpler expressions in 1D and 2D. The energy density (6) and baryon-number density (7) are then inserted into the grand-canonical partition function (8).

B. Partition Function

In order to study the thermodynamics of a theory, we must construct a partition function. We shall discuss both grand-canonical and canonical partition functions, which are also discussed in Refs. [23, 24]. The explicit expressions for the thermodynamic partition functions will be given for the baby-Skyrme and the Skyrme models. The Metropolis principle is used to evaluate the partition functions, see Refs. [23, 24] for more details.

1. The Grand-Canonical Partition Function

The general thermodynamic partition function for a general unitary field theory on the lattice is given by

$$\begin{aligned} \mathcal{Z} &= \int \prod_{p=1}^{M^d} d^{d+1} \phi_p d^{d+1} \dot{\phi}_p \delta(\dot{\phi}_p \cdot \phi_p) \delta(\phi_p^2 - 1) \\ &\quad \times \exp(-\beta(E - \mu B)) , \end{aligned} \quad (8)$$

where an integration is to be performed over the field and field derivative at each lattice point. The quantities E and B are the total energy and baryon number of the system.

If the field makes small vibrations (which must be harmonic) at each lattice point then each degree of freedom contributes $\frac{1}{2} k_B T$ to the free energy. There are M^d lattice sites, each with d potential and d kinetic degrees of freedom. The total energy due to lattice vibrations is thus $E_{\text{vib}} = \frac{2dM^d}{2\beta}$. The energy due only to solitons,

which we shall refer to as the scaled energy, is

$$E_{\text{scaled}} = E_{\text{total}} - E_{\text{vib}} = E_{\text{total}} - \frac{dM^d}{\beta} . \quad (9)$$

It is clear that these vibrational contributions are unphysical and need to be removed, since in the continuum limit their contribution would become infinite. The sine-Gordon model is renormalisable, and by subtracting the energy due to the lattice vibrations, we obtain the contribution due entirely to the solitons in a similar way as was done analytically in Ref. [17]. The baby-Skyrme and Skyrme models are non-renormalisable, and we find that it is therefore not possible to remove all the lattice-dependency from the energy expression. However, by removing the harmonic contribution, the lattice-dependency is reduced. We will not use the energy of a system to examine phase transitions, because of these lattice-dependencies. Instead, we use other, less lattice-dependent methods, which we will discuss in Secs. III B and III C.

It is useful to use density-like quantities rather than total quantities, and therefore we often use quantities like the average potential-energy density $\mathcal{V} = \frac{V}{h^d M^d}$ and the average baryon density $\mathcal{B} = \frac{B}{h^d M^d}$, where $h^d M^d$ is the volume of the system. Results are even more comparable when measuring $\frac{\mathcal{V}}{\mathcal{B}}$ (or $\frac{V}{B}$), which gives the potential energy per soliton. By measuring density-like quantities, we are measuring quantities which remain finite and meaningful in the limit of an infinite simulation volume.

The chemical potential μ determines the particle density in a particular system. We initially expected that a simulation of the grand-canonical partition function automatically includes the probability of adding or removing a soliton from the system. Unfortunately, because we are working with extended particles, a soliton can only be added or removed from the system if a number of field vectors on our discretised lattice change simultaneously. The probability of this happening is extremely small, and has never been observed in our simulations. The only examples of the total particle number changing is if the numerics become unstable. In this case, neighboring vectors are pointing in quite different directions such that the derivatives, and therefore the energy and baryon densities, are not calculated correctly. The numerical breakdown, i.e. the unphysical loss of winding number, is dependent on the lattice spacing, because it occurs at lower densities and temperatures if the lattice spacing is increased. Such numerical breakdown must occur when we have less than the minimum number of lattice points that can describe a Skyrmion.

To solve the problem that the number of particles in a given simulation is fixed by the topology, we use an open system, where particles can flow through the boundaries freely and therefore we have a heatbath that acts as a source of particles. The method we use to implement our open system will be discussed in Secs. III B, and III C, when we discuss the thermodynamics of our soliton models.

2. The Canonical Partition Function

The canonical approach is usually applied to a closed system, i.e. where particles are trapped in a box, and the number of particles in this box remain constant. As already mentioned in the last section, the number of solitons is conserved by the topology of the system. Therefore, the canonical approach seems to be very suitable to investigate the thermodynamics of soliton systems. The average density of particles is therefore defined by the initial choice of the number of particles B in the volume V and it never changes throughout the simulation. We choose not to implement fixed boundaries, which have the vacuum value on the simulation edges, but instead we use periodic boundaries. A system with periodic boundaries can be interpreted as an approximation of an infinite system because the simulation box is effectively duplicated an infinite number of times. Periodic boundary conditions imply that if a Skyrmion flows through one boundary of the simulation, then it reappears through the opposite side. Periodic boundary conditions have two advantages over fixed boundaries; firstly that the simulation can be interpreted as an infinite system, and secondly that we avoid unphysical boundary effects occurring from Skyrmions interacting with the fixed boundaries.

The general expression for the canonical partition function is

$$\mathcal{Z}_B = \int \prod_{p=1}^{M^n} d^{n+1}\phi_p d^{n+1}\dot{\phi}_p \delta(\dot{\phi}_p \cdot \phi_p) \delta(\phi_p^2 - 1) \times \exp(-\beta E), \quad (10)$$

where all the symbols are again defined as in Sec. II B 1. The harmonic contributions to the potential energy are removed in a similar manner as for the grand-canonical approach,

$$V_{\text{scaled}} = V_{\text{total}} - \frac{nM^n}{2\beta}. \quad (11)$$

In Ref. [24] the zero-temperature minimal-energy solutions are calculated using simulated annealing

within the canonical approach. For such static solutions, a renormalisation is irrelevant. Furthermore, the kinetic energy is irrelevant since the total energy is equal to the potential energy.

We now use the fact that $\dot{\phi}$ is an eigenvector of the mass matrix (4) to perform the integral over $\dot{\phi}$ analytically. The partition function now simplifies to

$$\mathcal{Z} = \mathcal{N}^{-1} \beta^{-\frac{dM^d}{2}} \int \prod_{p=1}^{M^d} d^{d+1}\phi_p \left(\sqrt{\frac{1 + \partial_i \phi_{c,p} \partial_i \phi_{c,p}}{\det(\mathcal{M}_p)}} \right) \times \exp(-\beta(V_p - \mu B_p)), \quad (12)$$

where V_p and B_p are the potential energy and baryon number at the lattice site p and represent the potential energy and baryon number in the surrounding unit cell. The overall constant factor \mathcal{N}^{-1} is irrelevant when applying the Metropolis principle, and will be ignored from now on. Eq. (12) will therefore be used as the grand-canonical partition function. The lattice does not need to be cubic, but we have adopted the convention that all the sides have equal length in order to avoid the additional notation required when using unequal lengths.

The procedure discussed above can be applied to the canonical formalism, and as expected we obtain the expression (12) with $\mu = 0$.

The partition function (12) cannot be evaluated analytically, and therefore a Metropolis algorithm is applied, see Refs. [23, 24] for more details.

The only exception is the sine-Gordon model. The grand-canonical partition function is derived in Ref. [17]. It can very easily be compared to our simulations, since it is obtained by discretising the field and then taking the continuum limit. Like many other field-theory models, the observables tend to infinity as the continuum limit is being reached. It thus illustrates clearly the role of renormalisation.

The canonical partition function of the sine-Gordon model in the angle representation is given by

$$\begin{aligned} \mathcal{Z}_B &= \int \prod_{p=1}^M d^2\alpha_p d^2\dot{\alpha}_p \exp\left(-\beta\left(\frac{1}{2}\partial_t\alpha_p\partial_t\alpha_p + \frac{1}{2}\partial_x\alpha_p\partial_x\alpha_p + 1 - \cos\alpha_p\right)h\right) \\ &= \text{const} \sqrt{\frac{1}{\beta}} \int \prod_p d^2\alpha_p \exp\left(-\beta\left(\frac{1}{2}\partial_x\alpha_p\partial_x\alpha_p + 1 - \cos\alpha_p\right)h\right), \end{aligned} \quad (13)$$

where α is the field, and $\sqrt{\frac{1}{\beta}}$ originates from evaluating the time derivative analytically, see Sec. II B 1. The

lattice spacing h is required to convert the energy density to the energy in a cell from the discrete lattice. The constant factor in the expression for \mathcal{Z}_B is irrelevant when

measuring thermodynamic quantities, and is therefore set equal to one. The reason every lattice point behaves like a classical harmonic oscillator is that the kinetic energy and potential energy are quadratic in time derivatives and spatial derivatives, respectively. The contribution to the fluctuations at individual lattice points from the potential $1 - \cos(\alpha)$ is negligible. The energy at a single lattice point due to fluctuations in the field is given by $\frac{(\alpha_{i+1} - \alpha_i)^2}{2h^2} \times h$, or $\frac{(\alpha_{i+1} - \alpha_i)^2}{2h}$, where i is the lattice index and h is the lattice spacing. Therefore,

$$\begin{aligned} \mathcal{Z}_B &= \left(\frac{2\pi}{\beta}\right)^{M/2} \int \prod_{i=1}^M \exp\left(-\beta \sum_i \frac{(\alpha_{i+1} - \alpha_i)^2}{2h}\right) \\ &\quad \times d\alpha_1 \dots d\alpha_M \\ &\approx \left(\frac{2\pi}{\beta}\right)^{M/2} \left(\frac{\text{const} \times h}{\beta}\right)^{M/2}. \end{aligned} \quad (14)$$

Using $P = \frac{1}{\beta L} \frac{\partial \mathcal{Z}_B}{\partial \beta}$, the harmonic oscillator contribution to the pressure becomes $P = \frac{M}{L\beta} \ln\left(\frac{\text{const} \times h}{\beta}\right)$. Since the harmonic oscillator at every lattice point gives a finite contribution to the pressure P , it becomes infinite in the continuum limit. The constant is not evaluated explicitly here because its contribution to the energy which we are interested in is irrelevant. Furthermore, the lattice spacing h within the logarithm also vanishes. The energy becoming infinite in the continuum limit can be overcome by removing the contribution from the harmonic oscillators. This way, all quantities are calculated without contributions from the harmonic oscillators, and contain only contributions that are not divergent in the thermodynamic limit. Therefore, the pressure due entirely to the solitons is given by

$$P' = - \left(\frac{A\left[-\frac{i\mu\beta}{\pi}, 4\beta^2\right]}{8\beta^2} + 1 \right). \quad (15)$$

We find that the density and internal-energy density for a given β and μ , which are obtained by using the standard thermodynamic relationships [25, 26] $\rho = \left(\frac{\partial P}{\partial \mu}\right)_\beta$ and $u = -\left(\frac{\partial(P\beta)}{\partial \beta}\right)_{\mu\beta}$ respectively, are

$$\rho = -\frac{1}{8\beta^2} \frac{\partial A\left[-\frac{i\mu\beta}{\pi}, 4\beta^2\right]}{\partial \mu} \quad (16)$$

and

$$u = \left(\frac{\partial \left(\frac{1}{8\beta} A\left[-\frac{i\mu\beta}{\pi}, 4\beta^2\right] + \beta \right)}{\partial \beta} \right)_{\mu\beta}. \quad (17)$$

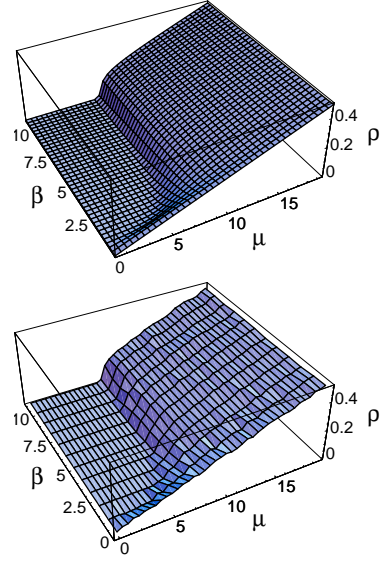


FIG. 1: The exact (top figure) and numerical (lower figure) results for the grand-canonical equation of state of the sine-Gordon model.

III. RESULTS

A. Sine-Gordon model

A check of the calculations can be made by comparing the exact results as discussed in the previous section to a calculation using open boundary conditions. This means that we impose no boundary conditions at all on the finite simulation volume, but allow solitons to enter the system through those boundaries. Even though, in principle, one can create topological charge on a grid, in practice topological charge is very well conserved. The only way to perform a grand-canonical simulation in practice is thus using open boundary conditions. We then compare the simulated result for the density of solitons to the analytic result, Eq. (16), in Fig. 1 as a function of β and μ . As we can see the results are very similar, with some statistical noise in the simulated results. Since it is much more straightforward to perform large simulations for the sine-Gordon model than for the 2D and 3D Skyrme models, this shows the best quality of results that can be expected (apart from a limitation in simulation time, since we have looked at quite a dense set of grid for the results).

B. Thermodynamics of the Baby-Skyrme Model

1. The Grand-Canonical Approach

The special feature of the grand-canonical approach is that we use open-boundary conditions. This means that the number of particles present in a particular simulation can change when particles enter or leave the system over the boundary. The lattice points at a boundary behave

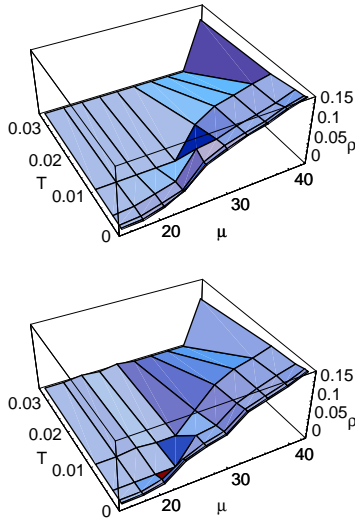


FIG. 2: The μ , ρ , T phase portrait for the baby-Skyrme model. *Top*: The order in which the points in the plot are calculated is in the increasing T direction with constant μ . *Bottom*: The calculation order is in the decreasing T direction with constant μ . The plots differ because the initial field configuration at each point is the final configuration of the previously calculated point. The axes are labeled in Skyrme units.

slightly differently than the internal ones. If a field vector is sampled at a boundary, it is accepted or rejected depending only on the change in the integrand on the neighboring internal plaquettes (we use the word plaquette for a square enclosed by four nearest neighbor lattice points). The field vectors at the boundaries are therefore less restricted than those at other lattice points.

The μ , ρ , T phase diagram for the baby-Skyrme model shown in Fig. 2. Each point is a separate simulation which has reached equilibrium for a given chemical potential μ and a temperature T . To save computing time, the initial field configuration used to calculate the density ρ at each point in the plot was the final configuration for the previously calculated temperature. The arrows in Fig. 2 show the order the simulations were calculated in. Two plots of the same phase portrait have been shown where the order of calculation has been reversed. The reason for showing this is because the computing time required to reach equilibrium becomes large near the phase transition, and the simulation time was not long enough to reach equilibrium near the phase transition. By comparing the two graphs, one can see that it is difficult to predict the chemical potential of the transition to within 5 Skyrme-energy units per soliton. In Fig. 3, the net density of baby-Skyrmions ρ is shown against the chemical potential μ at a fixed temperature T , for two different temperatures. In each plot, the order in which μ changes has been shown; one in the increasing μ direction and one in the decreasing μ direction. For low temperatures, the

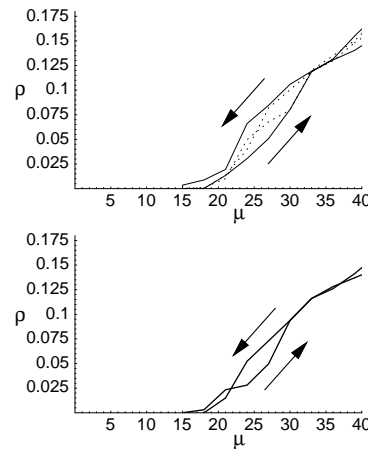


FIG. 3: The hysteresis effect when increasing and then decreasing the chemical potential μ . *Top*: The solid lines, where the arrows mark the direction of the simulation, show the hysteresis effect for a low temperature $T = 0.0001$. The dashed lines are the results imported from Fig. 2, where the temperature was changed for constant μ . *Bottom*: For higher temperatures, the hysteresis effect is less visible. The axes are labeled in Skyrme units.

hysteresis effect is more visible than for higher temperatures, because solitons do not move as quickly and hence it takes longer to reach equilibrium. The magnitude of the hysteresis effect depends on the computing time used, as equilibrium is reached extremely slowly and we did not have the time to let the system strictly reach it.

Each baby-Skyrmion has to have an energy greater than the topological lower bound for it to exist in an open system simulation. Fig. 3 shows that the chemical potential, which defines how much energy is given to each soliton, must be greater than approximately 18 Skyrme-energy units per baby-Skyrmion, $\mu \gtrsim 18$. Once the chemical potential is greater than the threshold, the density increases approximately linear with the chemical potential, $\rho \propto \mu - \mu_{\text{threshold}}$.

As long as μ is large enough, which is the case for almost all of the finite- ρ region, the state of the system is crystalline. The open boundaries allow crystal structures to form without defects, and therefore we can determine the “natural” crystal structure which will be described in the next section. The liquid state and the phase coexistence between solid and vacuum states exist near the phase transition and are too difficult to model using the grand-canonical approach. These states will be examined using the canonical approach in Sec. III B 2.

For high densities and low temperatures, the Skyrmions merge into a lattice where it is not possible to identify individual Skyrmions, see Fig. 4. Since there are no fixed boundaries in this simulation, there are no defects in the crystalline solutions either. The lattice is determined most easily from the structure of the “holes” with zero baryon-number density. There are two such minima present per baryon. In this crystal phase, the

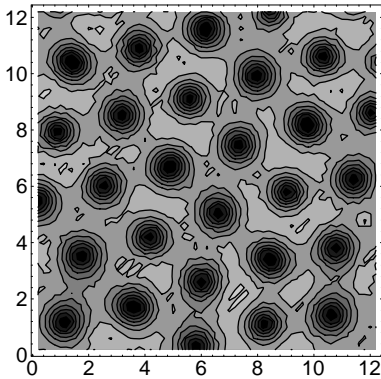


FIG. 4: Baryon-number density plots of the natural crystal structure of the baby-Skyrme model with open-boundary conditions. The baryon-number density is averaged over 20000 steps. The axes are labeled in Skyrme-length units. Lighter shades represent higher baryon-number densities. The parameters for this simulation are $\mu = 30$, $T = 0.05$, and the number of solitons in the simulation volume is about 13 ($\rho = xxx$).

average field $\langle \phi \rangle$ is zero, and therefore a mean-field chiral symmetry exists.

The triangular nature of the crystal is evidence that the type of crystal favored by the baby-Skyrme model is independent of the lattice used to discretise the model. Even though the lattice is square, the crystal which forms does not align itself to it. Since this simulation allows the crystal structure having the lowest energy per baryon to form without being effected by boundary conditions, we call it the “natural” crystal structure. The field configuration within a unit cell was copied (since it satisfies periodic boundary conditions) and simulated annealing with periodic boundary conditions was used to accurately investigate the zero-temperature properties.

The correct high-density structure [20] where Skyrmions merge into a lattice is shown in Fig. 5. The lattice is determined most easily from the structure of the “holes” with zero baryon-number density, since it is not possible to identify individual Skyrmions. There are two such minima present per baryon. In the low-density phase, the average field $\langle \phi_k \rangle$ is polarized in the direction of the sigma field, but for high densities, the average field is zero. Therefore, a mean-field chiral symmetry exists in the high-density phase and not in the low-density phase. The energy per baryon ratio when minimizing the energy of a field configuration having the form of the natural crystal is 18.27 Skyrme-energy units at a density of 0.024 particles per cubic Skyrme-length unit. If the density is lowered further, then the minimal-energy solution consist of small numbers of Skyrmions bound together, i.e. the multi-Skyrmions. In fact, this can be defined as the point where the phase transition between the high-density and low-density matter occurs.

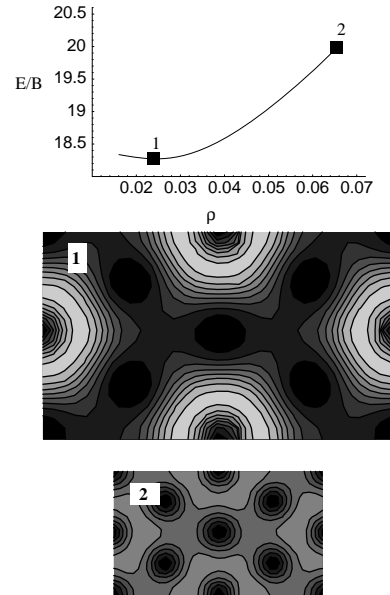


FIG. 5: The high-density phase at zero temperature. *Top*: Energy per baryon against density. *Middle*: A baryon-number density plot of the lowest energy per baryon number attainable, i.e. the “natural” crystal structure. Lighter shades represent higher baryon-number density. *Bottom*: A baryon-number density plot at high density. The baryon number is more evenly distributed throughout the structure. The middle and right plot are drawn to the same scale.

2. The Canonical Approach

As we have argued before, with periodic boundary conditions it seems impossible to generate additional topological charge. Nevertheless these calculations are much preferable over the open boundary calculations, since the results suffer much less from artifacts due to those boundaries (but the results will now depend much more strongly on the symmetries of the initial seed to the simulation). This is still the preferred way to calculate the phase diagram. In order to create the ρ , T , $\frac{u}{\rho}$ phase diagram, the lattice-dependent terms must be removed from the internal energy. Unfortunately, the lattice-dependency cannot be removed entirely, because the baby-Skyrme model is non-renormalisable.

The internal energy per unit area u is found by using the thermodynamic relationship

$$u = U/L^2 = -\frac{1}{L^2} \left(\frac{\partial \ln \mathcal{Z}}{\partial \beta} \right)_B, \quad (18)$$

where L^2 is the simulation volume and B denotes the constant particle number defined by the initial conditions. Therefore,

$$u = \frac{M^2}{L^2\beta} + \frac{1}{L^2} \frac{\int \prod_p d^3\phi_p \left(\sqrt{\frac{1+\partial_i\phi_{c,p}\partial_i\phi_{c,p}}{\det(\mathcal{M}_p)}} \right) V_p \exp(-\beta(V_p))}{\int \prod_p d^3\phi_p \left(\sqrt{\frac{1+\partial_i\phi_{c,p}\partial_i\phi_{c,p}}{\det(\mathcal{M}_p)}} \right) \exp(-\beta(V_p))} = \frac{1}{h^2\beta} + \frac{1}{L^2} \langle V \rangle, \quad (19)$$

where h is the lattice spacing and $\frac{1}{L^2} \langle V \rangle$ is the potential energy per unit area.

One can attempt to remove some of the lattice-dependency by assuming that the fluctuations at lattice points behave like harmonic oscillators, and therefore assuming that the contribution from the potential energy of the harmonic oscillator, $\frac{1}{h^2\beta}$, can be removed, so

$$u_{\text{scaled}} = \frac{1}{L^2} \langle V \rangle - \frac{1}{h^2\beta}.$$

Unfortunately u_{scaled} still depends strongly on the lattice spacing. Furthermore, for high temperatures, u_{scaled} can become negative, making its interpretation difficult. If the number of solitons in the system is zero, u_{scaled} still has a non-linear behavior that can become negative, when we would expect it to be zero. This is clearly an indication of the non-renormalisability of the Skyrme model, and we can no longer use the simple technique (count the lattice degrees of freedom) used to renormalise the sine-Gordon model

Instead of searching for a detailed theoretical explanation of the lattice-dependency, which would require the study of counter terms, we chose to compare simulations with a fixed number of solitons with simulations that use the same lattice parameters and are at the same temperature, but contain zero solitons. Thus, we use

$$u_{\text{scaled}} = \frac{1}{L^2} \langle V \rangle - \frac{1}{L^2} \langle V_0 \rangle, \quad (20)$$

where $\langle V \rangle$ is the potential energy of a simulation with solitons, and $\langle V_0 \rangle$ is the potential energy of the same simulation without any solitons. Although there is still some lattice-dependency, it is not very strong. It is likely that it is not possible to completely remove the dependency on the lattice spacing because the model is non-renormalisable. Nonetheless, we use this method because the internal energies for different lattice spacing become quite comparable, and phenomena such as phase transition points do not seem to depend on the lattice scale chosen.

We first use a canonical approach to study the ρ , T , $\frac{u}{\rho}$ phase diagram. The internal energy per soliton is plotted against the density ρ and the temperature T in Fig. 6. The internal energy is measured using Eq. (20). The density ρ is altered by changing the lattice spacing h while keeping the number of Skyrmions in the system at a constant value. Although Eq. (20) is used to remove some of the lattice-dependency, there is still a remaining contribution.

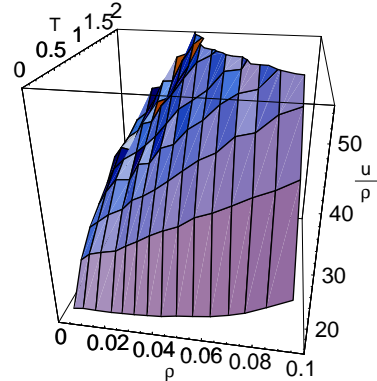


FIG. 6: The ρ , T , $\frac{u}{\rho}$ phase diagram. Some of the contribution from finite-lattice effects is removed by using Eq. (20) to find the internal-energy density. The density ρ is altered by changing the lattice spacing and keeping the same number of Skyrmions in the system. The axes are labeled in Skyrme units. (16 solitons on a 90×90 lattice.)

At finite temperatures, vibrations at each lattice point are present, but the contribution to the energy depends on the number of lattice points per volume. Since we vary the lattice spacing to change the soliton density, the internal energy per soliton as shown in Fig. 6 may not be properly compared for different densities. This phase diagram will not be discussed further, because it cannot be used to interpret the states of matter throughout the ρ - T plane. In the next two sections, the methods that successfully determine the states of matter for the baby-Skyrme model throughout the ρ - T plane are discussed.

Along the lines first proposed by Klebanov [27], we analyse the grid-averaged fields $\langle \phi \rangle$. The average of the pion fields $\langle \pi \rangle$ is always zero, but the average sigma field $\langle \sigma \rangle$ changes. The average sigma field $\langle \sigma \rangle$ is plotted against the temperature T and the density ρ in Fig. 7.

When few Skyrmions exist in a large volume, $\langle \sigma \rangle > 0$. This is because the vacuum, where $\sigma = 1$, contributes a significant amount to the average sigma field. For high densities, however, the baby-Skyrmions combine in such a way that the individual baby-Skyrmions cannot be identified. Furthermore, an approximately chirally-symmetric configuration is formed where $\langle \sigma \rangle \approx 0$ and the sigma field and the pion fields are interchangeable without change in energy. For the baby-Skyrme model, chiral symmetry is never exactly satisfied (in a time average), because the pion-mass term, which is required to stabilize the solitons, violates this symmetry. As the density of a system is increased, $\langle \sigma \rangle = 0$ is approached

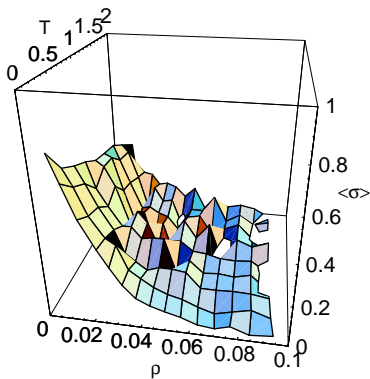


FIG. 7: The chiral symmetry (magnetization) $\langle\sigma\rangle$ as a function of ρ and T . For fluids and solids, we find $\langle\sigma\rangle \approx 0$. For the phase coexistence between solid and vacuum, $\langle\sigma\rangle > 0$. T and ρ are given in Skyrme units and $\langle\sigma\rangle$ is dimensionless. The parameter $\langle\sigma\rangle$ has been measured from a single field configuration and has not been averaged through time, and the results show large fluctuations. All simulations were performed for 16 solitons on a 90×90 lattice, and the density was varied by changing the lattice spacing.

asymptotically. In Fig. 7, a phase transition in $\langle\sigma\rangle$ can be observed to occur between the densities $0.02 < \rho < 0.04$ for various temperatures.

The fluctuations in $\langle\sigma\rangle$ are largest in the region $0.02 < \rho < 0.08$, $T > 0.5$. In the next section, we identify a liquid and a solid phase in the chirally symmetric phase, and the liquid region is located where the fluctuations in $\langle\sigma\rangle$ are largest. The liquid and solid states possibly extend into the broken chiral symmetry phase, depending on where one defines the chiral phase transition to be. These fluctuations are present because in Fig. 7 $\langle\sigma\rangle$ was calculated from a single field configuration and not averaged in time. Also, the $\langle\sigma\rangle$ phase portrait seems to be independent of the lattice parameters, unlike the internal-energy density. When doubling the number of lattice point and keeping the same number of baby-Skyrmions in the same volume, the $\langle\sigma\rangle$ phase diagram is not significantly different than the one shown in Fig. 7.

By examining the pseudo-time-averaged baryon-density plots at various temperatures and densities, one can easily identify three different states that a particular simulation may be in, namely in a solid, in a liquid, or in a phase-coexistence state. Furthermore, correlation functions may be used to draw the same conclusions. In this section, the number of solitons in a system is varied to create different densities, while the lattice size and the lattice spacing remain fixed. Although the results shown have the same lattice parameters, the same conclusions can be drawn in simulations with different lattice parameters, as has been checked for a number of examples.

An example of the baryon-number density distribution for a solid is given in Fig. 8. On the left we show a pseudo-time-averaged baryon-number density plot and on the right a snapshot where thermal fluctuations are evident. The approximate triangular crystal structure

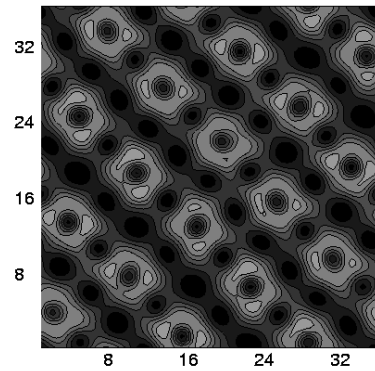


FIG. 8: A simulation in the solid phase. Pseudo-time-averaged baryon-number density plot. Lighter shades represent higher baryon-number density and the units shown are in Skyrme-length units. The density $\rho = 0.04$, which implies that each light-colored circle contains two units of topological charge.

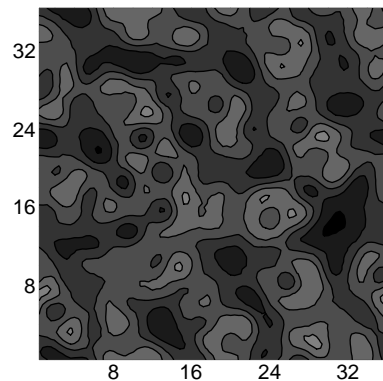


FIG. 9: A simulation in a liquid phase, as a pseudo-time-averaged baryon-density plot with an average taken with 2000 pseudo-time steps. The shades from dark to light represents low to high baryon-number densities and the units shown are in Skyrme-length units. As in Fig. 8 $\rho = 0.04$, but the temperature is higher.

can be observed although defects are present, which are a consequence of using periodic boundary conditions, in contrast to the absence of defects seen when using the grand-canonical approach.

A pseudo-time-average of a liquid shows an almost constant baryon-number density, because structures move, see Fig. 9. The visible structure in a pseudo-time-averaged baryon-density plot is dependent on the number of iterations used to create it, in this case 2000 pseudo-time steps.

In the phase-coexistence region, one observes series of multi-solitons that do not change with pseudo-time, i.e. a solid structure surrounded by large regions of vacuum. These can either be interpreted as a crystal of nuclei, or as a percolating network. An example is shown in Fig. 10.

The solid, liquid and phase-coexistence states can also be identified by examining correlation graphs. The cor-

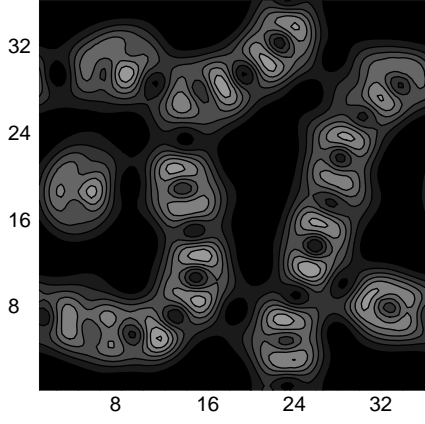


FIG. 10: Pseudo-time averaged baryon-number density plot in the phase-coexistence region. The shades from dark to light represents low to high baryon-number densities. As in Figs. 8,9 $\rho = 0.04$, but the temperature is intermediate between the two.

relation graphs are created by plotting the correlation between the baryon number at the lattice points,

$$C(r) = \sum_{a=1}^{\text{all lattice points}} \sum_{b=1}^{\text{all lattice points}} (\langle B_a^2 B_b^2 \rangle - \langle B_a^2 \rangle \langle B_b^2 \rangle) \times \delta(r - |\mathbf{r}_a - \mathbf{r}_b|), \quad (21)$$

against r , which is the separation between lattice points a and b . The correlation function C at r is calculated by taking the average of the correlation with respect to all a and b separated by a distance r . To keep track of the value $B_a^2 B_b^2$ for each separation distance, we bin the values, and therefore the distances are rounded to the nearest half-lattice spacing, i.e. to the nearest $h/2$.

The correlation graphs can be used to identify the state of a system. For solids and phase coexistence (which is a solid surrounded by vacuum), correlation functions show peaks a distance of several Skyrme-length units away from the origin, see Fig. 11. For liquids, however, the correlation function levels to zero quickly. The non-zero component is the correlation of Skyrmions with themselves, and is therefore non-zero for approximately the length of the radius of a baby-Skyrmion. Some structure is visible to a distance of 10 Skyrme-length units because interactions with neighboring Skyrmions are still present. It is because of the visible long-range interaction that we interpret the state to be a liquid rather than a gaseous state. The advantage of using correlation functions rather than pseudo-time-averaged baryon-density plots to identify liquids is that they are not dependent on the number of iterations used to create them.

The transition from solid to liquid as the temperature is raised at a constant density is shown in Fig. 12. Both the pseudo-time-averaged baryon-density plots and the corresponding correlation functions are shown to highlight the fact that the state of the system can be identified

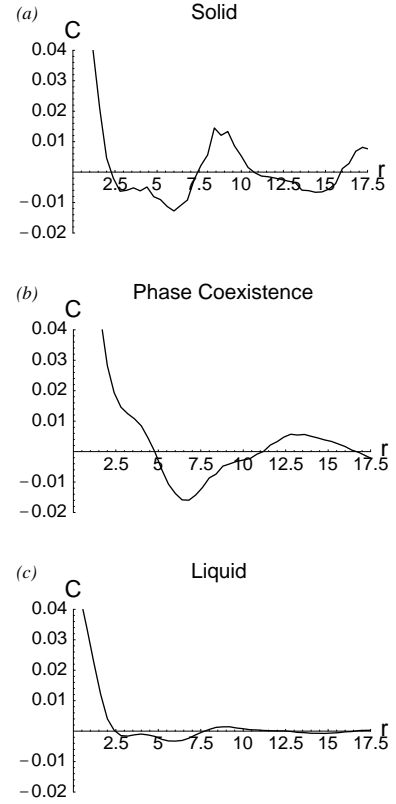


FIG. 11: The correlation functions for a solid, a state in phase coexistence, and a liquid, respectively. (a): For the solid, there are peaks a distance of several Skyrme-length units away from the origin because the crystal is repetitive. (b): For phase coexistence, there are also peaks a distance of several Skyrme-length units away from the origin because the baby-Skyrmions are bound together, but the peaks are weaker than for a simulation in the solid phase, and lack the fine structure. (c): For a liquid, the correlation function decreases rapidly to zero after a few Skyrme-length units. The non-zero component exists because of the correlation of Skyrmions with themselves. (r is in Skyrme-length units and C is dimensionless.)

through either method. The simulations whose baryon densities are plotted on the left have all been identified as solids and those plotted on the right have been identified as liquids. The pseudo-time average for these plots was set to 2000 iterations, and therefore it can be seen that the baryons move around more for simulations at higher temperature. When using more iterations, the baryon density approaches the average everywhere, but because there is less structure, it defeats the purpose of these illustrations. It is not possible to identify the structure at $T = 0.2$ directly from the baryon-density plot, but the correlation function clearly shows that it is a solid. The apparent motion of the solitons are lattice vibrations.

Fig. 13 shows the final phase portrait for the baby-Skyrme model which has been created by examining the pseudo-time-averaged baryon-density plots and correlation functions at various temperatures and densities. We identify solid, liquid, and phase-coexistence regions, by

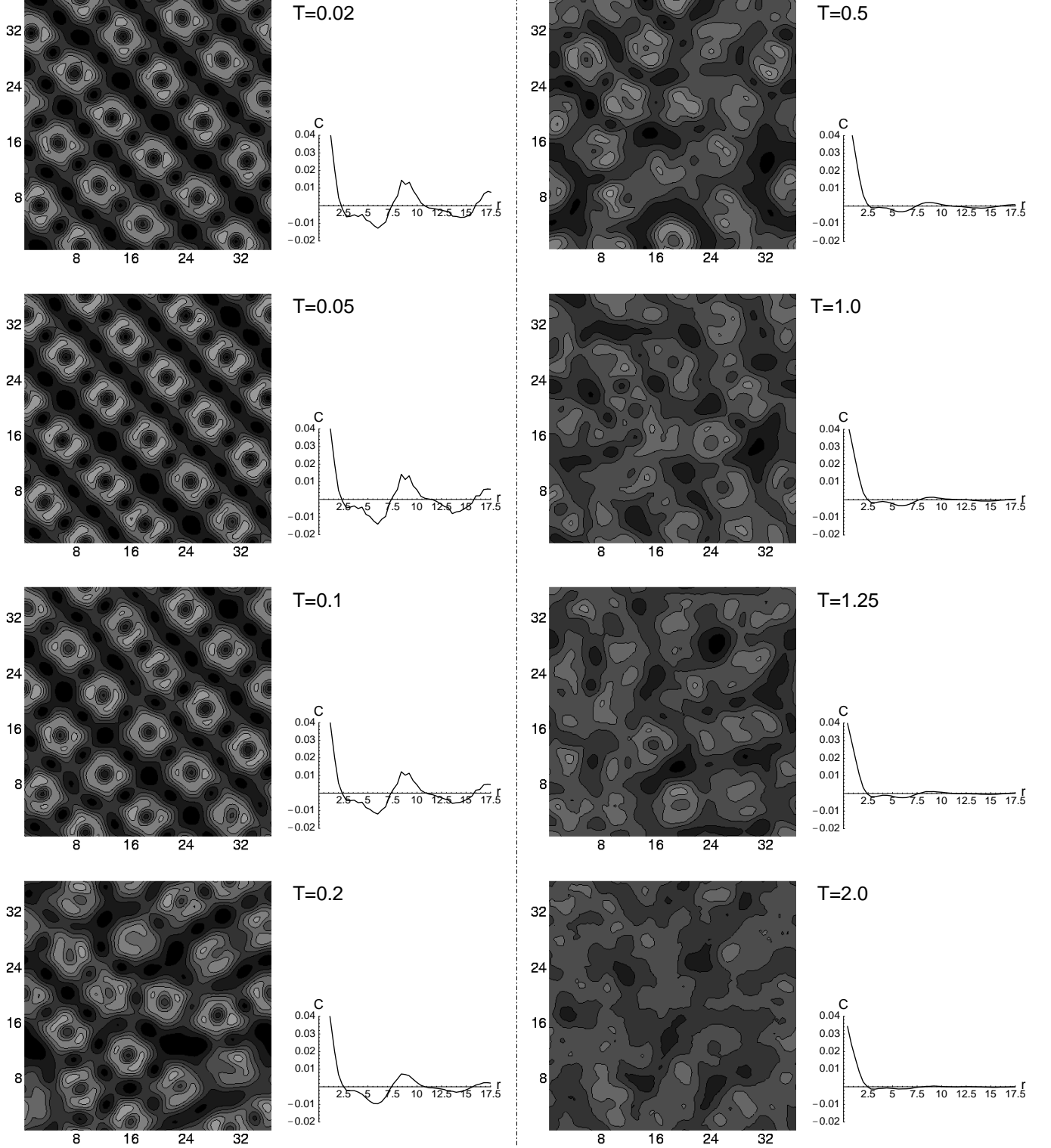


FIG. 12: Pseudo-time-averaged baryon-density plots and the corresponding correlation functions for various temperatures with density $\rho = 0.028$. The length units shown are in Skyrme-length units and the correlation units are dimensionless. The contour levels for all plots are identical where white illustrates the highest baryon density. All simulations are performed on a 90×90 size lattice with lattice spacing $h = 0.4$. The simulations whose baryon densities are plotted on the left have all been identified as solids and those plotted on the right have been identified as liquids.

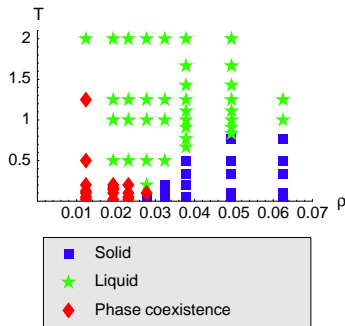


FIG. 13: The phase diagram. All plotted points are results obtained from simulations performed on a 90×90 lattice with a lattice spacing of $h = 0.4$ Skyrme-length units. The axes are labeled in Skyrme units.

combining the correlation function measure with that of the time-averaged baryon density.

Unfortunately, we are unable to determine the order of any of the phase transitions. It is unlikely that any of them are of first order, because we would expect to see discontinuities in the ρ , T , $\frac{\mu}{\rho}$ and ρ , T , $\langle \sigma \rangle$ phase diagrams. Since higher-order phase transitions can only be identified by discontinuities in the n -th order derivative, we are unable to do so since the results presented here contain statistical fluctuations that are large enough such that such an analysis becomes too difficult.

3. Conclusions

The baby-Skyrme model shows a rich phase diagram. By examining the chiral symmetry, the time-averaged baryon-density plots, the snapshot baryon-density plots and the correlation functions, it was possible to identify the state of matter that exists for a given density and temperature. Although the model is non-renormalisable and the internal energies are dependent on the lattice parameters, all the other measured quantities used seem to be unaffected. Therefore, we are confident that the mapping of the phase portrait of the baby-Skyrme model is given to a reasonable accuracy.

A similar diagram will be created for the 3D Skyrme model, and the phase diagrams are expected to differ because the stabilizing terms have different forms. In particular, we would like to know at which temperatures and densities the phase transitions occur and compare these with putative QCD phase diagram such as those in Ref. [3].

C. Thermodynamics of the Skyrme Model

In the previous section, we have successfully investigated the phase portrait of the baby-Skyrme model. We observed solid states, liquid states, and phase coexis-

tence between solid and vacuum states. The internal energy, even after removing some of the lattice contribution, is still dependent on the lattice spacing because the baby-Skyrme model is non-renormalisable. However, by examining the chiral symmetry breaking, correlation functions, and baryon-density plots, we were able to determine the state of the system with methods that do not depend on lattice spacing. We will repeat the same type of analysis for the Skyrme model. Since the Skyrme model is often argued to be an approximation to QCD, the Skyrme phase portrait will be compared to other model of QCD (specifically Ref. [3], which was created using another model). The phase transition between nuclear matter and “quark” matter is of particular current interest.

Unfortunately, we were unable to apply the grand-canonical approach to the Skyrme model. If the initial condition is a vacuum throughout the simulation box, we do not observe solitons entering the system. Skyrmions are expected to enter the system if $\mu > 65$ Skyrme-energy units per soliton. Simulations for a number of choices of μ , T and h suffered from numerical breakdown, which was identified by neighboring field vectors pointing in almost opposite directions, where all derivative approximations underlying the lattice approach break down. Numerical breakdown seems to occur more easily for the Skyrme model than for the baby-Skyrme model, most likely because the model is more complex. In the cases where a numerical breakdown did not occur, the initial vacuum never changed. Either solitons could not flow over the boundaries, or we did not have the computational time required to observe any solitons entering the system.

The field configuration that gives the lowest energy per soliton that has yet been observed is given by Castillejo *et al* [28] and the energy per soliton is 3.8% above the topological lower bound. It is not clear whether this simple-cubic lattice in half-Skyrmions is the natural crystal structure. The periodic boundary conditions used in that reference favor this configuration. In fact, since we see that the baby-Skyrme model has a triangular pattern, we would expect that a hexagonal close-packed structure is a candidate for the natural crystal structure. We were not able to create a canonical simulation where we had the correct number of particles in a simulation box that was shaped to favor a hexagonal close-packed crystal. This does not imply that it is not the natural crystal structure, but instead it means that guessing the correct environment without knowing exactly what this crystal looks like is extremely difficult. The natural crystal structure cannot be identified from the canonical simulations either, because large simulation volumes are required, and we do not have the computational resources to do this for the Skyrme model. Because of the large simulation volume required to identify the natural crystal structure from a canonical simulation, we probably would not have discovered the triangular crystal for the baby-Skyrme model without using the grand-canonical

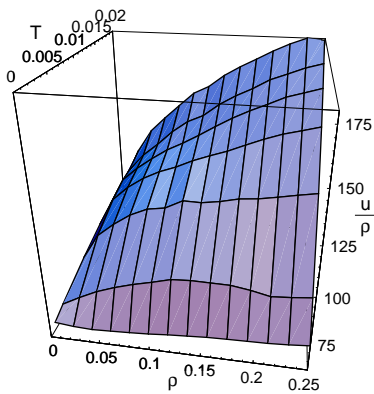


FIG. 14: The ρ , T , $\frac{u}{\rho}$ phase diagram. Some of the contribution from finite-lattice effects is removed by using Eq. (22) to find the internal-energy density. The density ρ is altered by changing the lattice spacing and keeping the same number of Skyrmions in the system. The axes are labeled in Skyrme units. (32 Skyrmions on an $80 \times 80 \times 80$ lattice.)

approach.

1. The Canonical Approach

The canonical approach for the nuclear-Skyrme model is implemented in a similar manner as for the baby-Skyrme model. Again, some of the lattice-dependency is removed from the internal energy. The internal energy of the solitons is given by

$$u_{\text{scaled}} = \frac{1}{L^3} \langle V \rangle - \frac{1}{L^3} \langle V_0 \rangle, \quad (22)$$

where $\langle V \rangle$ is the average potential energy of a simulation with finite density and inverse temperature β . The average potential energy $\langle V_0 \rangle$ is calculated from a simulation with identical parameters but without any Skyrmions, i.e. it is the potential energy due entirely to vibrations on the lattice.

The internal energy per Skyrmion is plotted against the density ρ and the temperature T in Fig. 14. The density ρ is determined by altering the lattice spacing h in a simulation with 32 Skyrmions on an $80 \times 80 \times 80$ lattice. Since some lattice-dependency is still present in the internal energy of the system, the internal energies at different densities may not be comparable, as they have been determined with different lattice spacings. It is not possible to determine the states of matter from Fig. 14, and therefore alternative methods will be used in the following sections.

The average sigma field is plotted against the density ρ and the temperature T in Fig. 15. As already discussed in the previous section for the baby-Skyrme model, a chirally-symmetric phase exists at high densities, $\langle \sigma \rangle = 0$, and chiral symmetry is broken at low densities, $\langle \sigma \rangle > 0$. Although it is difficult to determine the position of the phase transition between low-density and

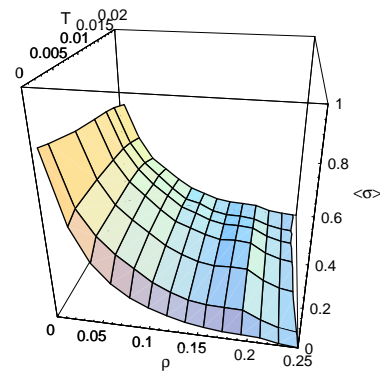


FIG. 15: The ρ , T , $\langle \sigma \rangle$ phase diagram. The kink is a signature of the phase transition between the low-density and high-density phases. The axes are labeled in Skyrme units. (32 Skyrmions on an $80 \times 80 \times 80$ lattice with varying lattice spacing.)

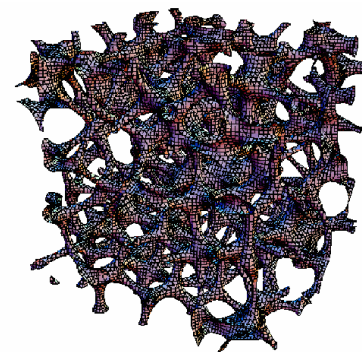


FIG. 16: A baryon-density contour plot, with a high baryon-density contour, of a simulation at a high density ($\rho = 0.244$ Skyrme-density units) and a finite temperature ($T = 0.2$ Skyrme-energy units). An irregular, but crystalline, structure can be seen. The mesh spacing is 0.08 Skyrme-length units. (64 Skyrmions on an $80 \times 80 \times 80$ lattice with volume 6.4^3 cubic Skyrme-length units.)

high-density matter precisely, we believe it occurs where a kink can be observed near $\rho = 0.2$ for all temperatures plotted in Fig. 15.

The pseudo-time-averaged baryon-density plots, with the help of correlation functions, can be used to identify the different states of matter. The solid, liquid and phase-coexistence states which are observed can then be used to determine the phase portrait for the Skyrme model. Since the Skyrme model is an approximation of QCD, the phase portrait we create can be compared to QCD.

Examples of a contour plot from a pseudo-time-averaged baryon-density distribution for a solid are shown in Fig. 16 for a high baryon-density contour. The crystal structure is irregular because the simulation volume of 6.4^3 cubic Skyrme-length units is too small and therefore defects are introduced. We expected to observe a hexagonal close-packed crystal of half-Skyrmions, but

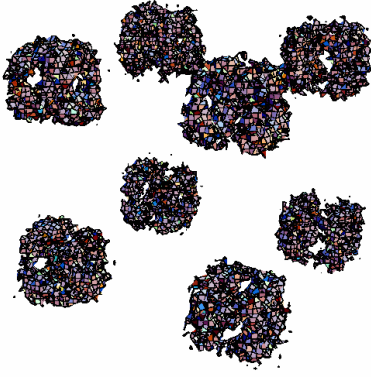


FIG. 17: A baryon-density contour plot of a simulation at a low density ($\rho = 0.122$ Skyrme-density units) and a finite temperature ($T = 0.2$ Skyrme-energy units). Eight $B = 4$ multi-Skyrmions can be seen with temperature fluctuations and they would look like the $B = 4$ multi-Skyrmions. The contour shown for each the $B = 4$ multi-Skyrmion has an approximate volume of 2.8 cubic Skyrme-length units. The mesh spacing is 0.08 Skyrme-length units. (32 Skyrmions on an $80 \times 80 \times 80$ lattice with volume 6.4^3 cubic Skyrme-length units.)

unfortunately no regular crystal can be identified. In a low-density contour plot [23], we observe that the low-density regions are all connected. This is in contrast to the disconnected circles of vacuum observed for the baby-Skyrme model.

We have not shown an example of a contour plot of the pseudo-time-averaged baryon-density distribution for a liquid. These look rather misleading when only one contour is shown, as regions with slightly higher- or lower-than-average baryon densities look like Skyrmions. These structures which are due to small differences in the pseudo-time-averaged baryon-number distribution are actually artifacts of the simulation process. When examining the results, we actually look at a variety of contours to verify that we have a liquid, but this would be too cumbersome to illustrate. A liquid can be distinguished from a solid most easily by observing that a liquid does not have connected low-density contours that look like tubes.

In the phase coexistence region, we observe multi-Skyrmions with large regions of vacuum surrounding them. An example is shown by a snapshot of a contour of the baryon-number distribution in Fig. 17. Here, eight $B = 4$ multi-Skyrmions can be seen. The $B = 4$ multi-Skyrmions are very tightly bound, like the alpha particles they model, which is why multi-Skyrmions of lower winding number are not seen. The boundary conditions also favor the $B = 4$ multi-Skyrmions over other multi-Skyrmions. Unfortunately, we are not able to run large enough simulations to see if a mixture of other multi-Skyrmions can be created. The regular spacing of the $B = 4$ Skyrmions is most likely also a consequence of a small number of Skyrmions in a limited simulation volume.

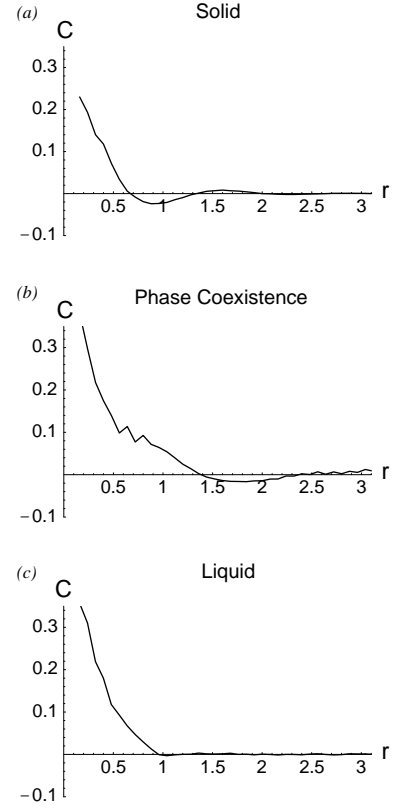


FIG. 18: The correlation functions for a solid, a state in phase coexistence and a liquid, respectively. (a): For a solid, the correlations show long-range order at large distances. The correlation function corresponds to the contour plots shown in Fig. 16. (b): For phase coexistence, the self-correlations of the $B = 4$ Skyrmions are clearly visible for $r < 1$. The correlation between the different $B = 4$ multi-Skyrmions can be seen for $r > 2.5$. (c): The function falls off faster than the function for the solid, but medium-range interactions are still present and therefore it is not identified as a gas. The correlation function corresponds to the contour plot shown in Fig. 17. (r is in Skyrme-length units and C is dimensionless.)

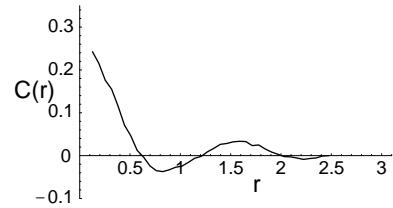


FIG. 19: The correlation functions for Castillejo *et al* crystal, which is identified as a solid. (r is in Skyrme-length units and C is dimensionless.)

The same correlation function that is used for the baby-Skyrme model can be applied to the Skyrme model, and has proven useful in the analysis of the results. The correlation functions for the solid, liquid and phase coexistence states are given in Fig. 18. The correlation functions seem to fall off faster for the Skyrme model than

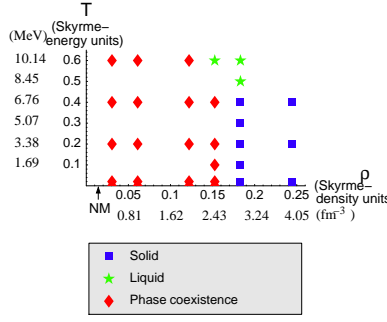


FIG. 20: The phase diagram of the Skyrme model including a pion-mass term. The density of nuclear matter (NM) is marked at 0.16 fm^{-3} . Other models predict the chiral phase transition at approximately 0.73 fm^{-3} [3]. All plotted points are results obtained from simulations performed on a $80 \times 80 \times 80$ lattice with a lattice spacing of $h = 0.08$ Skyrme-length units.

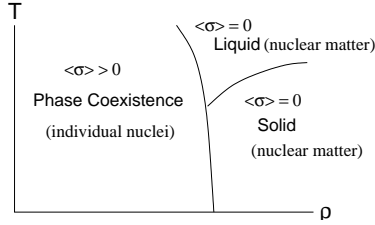


FIG. 21: A sketch of the phase diagram of the Skyrme model. The state of matter and chiral symmetry (or symmetry breaking) is marked. The corresponding phases of QCD are marked in parentheses.

for the baby-Skyrme model, but for solids and phase coexistence, a long-range order is clearly visible. The correlations for the putative solid must be compared to that of the parametrised solution by Castillejo *et al*, which consist of a simple cubic lattice of half-Skyrmions [28], is shown in Fig. 19. As one can see the decay of the correlation functions is very similar, if slightly less pronounced for the highly-defective solid found in our simulations. For liquids, there is also a visible medium-range order. The correlation of the $B = 4$ multi-Skyrmions with themselves and with other $B = 4$ multi-Skyrmions are clearly visible (at short and long distances respectively). Overall, the correlation functions for the Skyrme model show the same type of behavior as for the baby-Skyrme model.

The final phase portrait for the Skyrme model is shown in Fig. 20. The different states of matter were distinguished from each other by examining the pseudo-time-averaged baryon-density plots and the correlation functions. Classifying the different states of matter in the vicinity where the different phases meet is more difficult than for the baby-Skyrme model, because long-range correlations are not as distinct. This means that the assignments made at several points are somewhat ambiguous. Nevertheless, the approximate location where different phases meet has been identified. The chiral phase

transition also appears to separate the phase coexistence region with the liquid and solid regions for this model at $\rho = 0.18$ Skyrme-length units for the temperatures shown. Fig. 21 shows a sketch of the phase diagram and the states of matter and whether there is chiral symmetry is labeled. The solid and liquid phases are both chirally symmetric and are identified with the quark-gluon plasma. The coexistence phase is identified with nuclear matter. The phase transition observed from chiral symmetry breaking and the phase transition observed by looking at average baryon-density plots and correlation functions are not necessarily signatures of the same phase transition. If they are two different phase transitions, they are close enough together so that we could not resolve the two. Two different phase transitions may exist, because it may be possible to create crystals that break chiral symmetry which are not in phase coexistence with vacuum, which would be more identifiable with nuclear matter.

2. Conclusions and comparison with QCD

The phase portrait of the Skyrme model including a pion-mass term has been determined to a reasonable accuracy. The difficulties were mainly caused because each simulation required a significant amount of computing time. Furthermore, analysing three-dimensional structures also requires more time and effort. Unfortunately, we did not have the resources to extend the energy per baryon and chiral symmetry-breaking phase diagrams to higher temperatures.

We will now compare our results from investigating the Skyrme model at finite temperatures and finite densities to the phase portraits of QCD obtained by other models and illustrated in Sec. I. The phase transition between nuclear matter and deconfined quark matter occurs at $\rho = 0.18$ Skyrme-density units (2.9 fm^{-3}). This phase transition, which has the characteristic that chiral symmetry is broken, has been observed at $\rho = 0.045$ Skyrme-density units (0.73 fm^{-3}), which was obtained from Ref. [5]. The phase transition occurs at about 18 times the density of nuclear matter on earth of approximately 0.0099 Skyrme-density units (0.16 fm^{-3}) [29]. The lowest energy per baryon for QCD is most likely at the normal density of nuclear matter, because any excess energy would be radiated away. For the Skyrme model, the lowest energy per Skyrmeion occurs at 0.043 Skyrme-density units (0.70 fm^{-3}). The lowest energy per baryon for the Skyrme model and for QCD are not easily compared, because this value will change significantly when the Skyrme model is quantised.

The lowest temperature where a liquid phase is observed is at 0.5 Skyrme-energy units (8.45 MeV). Although this is approximately the temperature of the critical point where nuclear matter can continuously (i.e. without a phase transition) transform from a liquid to a gas, we believe that the lowest temperature where a

liquid can be observed should be identified with the temperature of the critical point where nuclear matter can transform to a quark-gluon plasma continuously. These critical points have been obtained from Ref. [3]. The reason we identify the lowest temperature at which a liquid is observed with the temperature of the critical point is because the high-density Skyrme matter, which behaves like a solid, is identified with the quark-gluon plasma, as individual Skyrmions are no longer distinct. The liquid phase may be the state where high-density Skyrme matter (quark-gluon plasma) can continuously be transformed to low-density Skyrme matter (nuclear matter). If this is the case, then the predicted temperature of the critical point is different by a factor of ten!

Alternatively, the liquid state for the Skyrme model may be identified with the liquid state for the quark-gluon plasma, because the liquid state observed for the Skyrme model is chirally symmetric. (Since there are not many samples for the nuclear-Skyrme model, we observe that this is also the case for the baby-Skyrme model.) If this is the case, we have not been able to heat simulations enough to reach the critical point. Furthermore, it is unclear whether the Skyrme model shows any observable phenomena there. Possibly there is a liquid state for all densities above this temperature.

The location of the phase transitions observed for the Skyrme model will not correspond exactly with those of QCD, because the Skyrme model is only a semi-classical approximation of QCD. However, it is difficult to model the different phases of QCD by using only one model. In future, the Skyrme model may be used to make statements about the order of phase transitions in QCD. We were not able to investigate this because we were only able to generate few samples (which each required a considerable amount of computation time) and even these samples are not statistically accurate enough to take derivatives of the phase spaces that were generated. We have, however, shown that field theories containing solitons have an interesting phase portrait.

IV. CONCLUSIONS AND OUTLOOK

The phase portraits for the baby-Skyrme and nuclear-Skyrme models were created accurately using the canonical approach. We have shown that the low-density and high-density phases can be distinguished through chiral symmetry breaking. Furthermore, pseudo-time-averaged baryon-density plots and correlation functions can be used to identify the state of matter at a given temperature and density. The baby-Skyrme model has a rich phase diagram. Although the model does not have a physical interpretation, we believe that similar phases exist for Skyrmions in the quantum Hall effect. The phase diagram for the nuclear-Skyrme model was compared to

other models of the QCD phase diagram. We were able to identify the phase where chiral symmetry is broken with hadronic matter and the chirally symmetric phase with the quark-gluon plasma. The location of the phase transition is at a higher density than predicted by other models. It remains unclear whether the boundary of the phase coexistence region with the liquid and solid regions occurs on the same line as the chiral phase transition.

The grand-canonical approach could not successfully be used to generate accurate phase portraits for the baby-Skyrme and nuclear-Skyrme models, but it is useful in determining the natural crystal structure for the baby-Skyrme model. The open boundaries in this approach allow crystals to form without defects. The grand-canonical approach is already being applied to QHE simulations [19]. Unfortunately, this method was unsuccessful for the nuclear-Skyrme model, partly because we did not have the necessary computer resources. We also were not able to run simulations for a large number of different parameters. We believe that it is possible to determine the natural crystal structure for the nuclear-Skyrme model, and therefore propose that this be attempted again. We suggest to remove the pion-mass term in such calculations, because the minimal energy per baryon occurs in the high-density phase rather than the low-density phase (as is the case when a pion-mass term is included). When using the grand-canonical approach, it may be effective to use an approximation to the derivative that results in overestimating the baryon number, rather than underestimating like we have done.

The thermodynamic investigations can also be applied for the Skyrme model with a sixth-order term and for the ω -stabilized Skyrme model. The higher-order terms become dominant at high densities, and may therefore be better models for describing such phases.

The nuclear-Skyrme model is a semi-classical approximation to QCD in the $N_c \rightarrow \infty$ limit. This approximation is not particularly accurate, but it means that a single model can be used to describe matter at both low densities and high densities. We were not able to investigate the order of the phase transitions, and since this may be relevant to QCD, it would also be interesting subject for future research.

Thus, we have derived methods to investigate models with soliton solutions for both zero and finite temperatures. The methods we developed can easily be applied to a wide range of similar models.

Acknowledgments

OS has been supported by an EPSRC studentship; NRW acknowledges support from the EPSRC through research grants GR/L22331 and GR/N15672.

-
- [1] I. Montvay and G. Münster, *Quantum Fields on a Lattice* (Cambridge University Press, Cambridge, UK, 1994).
 - [2] R. Gupta, *Introduction to Lattice QCD* (????), Lectures given at the *LXVIII* Les Houches summer school, "probing the standard model of particle interactions", July 28-Sept 5, 1997. hep-lat/9807028.
 - [3] K. Rajagopal, Nucl. Phys. A **661**, 150 (1999).
 - [4] M. Stephanov, K. Rajagopal, and E. Shuryak, Phys. Rev. Lett. **81**, 4816 (1998).
 - [5] J. Berges and K. Rajagopal, Nucl. Phys. B **538**, 215 (1999).
 - [6] M. A. Halasz, A. D. Jackson, R. E. Shrock, M. A. Stephanov, and J. J. M. Verbaarschot, Phys. Rev. D **58**, 096007 (1998).
 - [7] K. Rajagopal (2000), hep-ph/0005101v2.
 - [8] T. H. R. Skyrme, Nucl. Phys. **31**, 550 (1962).
 - [9] G. 't Hooft, Nucl. Phys. B **72**, 461 (1974).
 - [10] G. 't Hooft, Nucl. Phys. B **75**, 461 (1974).
 - [11] E. Witten, Nucl. Phys. B **223**, 433 (1983).
 - [12] E. Braaten and L. Carson, Phys. Rev. D **38**, 3525 (1988).
 - [13] E. Braaten, S. Townsend, and L. Carson, Phys. Lett. B **235**, 147 (1990).
 - [14] A. D. Jackson and J. J. M. Verbaarschot, Nucl. Phys. A **484**, 419 (1988).
 - [15] S. M. Girvin, in *Topological aspects of low dimensional systems. Les Houches lectures*, edited by A. Comtet, T. Jolicœur, S. Ouvry, and F. David (Springer Verlag, Berlin, 1998), vol. 29, p. 53, cond-mat/98.
 - [16] D. H. Lee and C. L. Kane, Phys. Rev. Lett. **64**, 1313 (1990).
 - [17] N. Gupta and B. Sutherland, Phys. Rev. A **14**, 1790 (1976).
 - [18] T. D. Cohen, Nucl. Phys. A **495**, 545 (1989).
 - [19] T. Weidig and N. R. Walet (2001), cond-mat/0106157.
 - [20] O. Schwindt and N. R. Walet, in *Intersections of Particle and Nuclear Physics*, edited by Z. Parsa and W. J. Marciano (AIP Conference Proceedings, Vol. 549, New York, 2000).
 - [21] O. Schwindt and N. R. Walet, Europhys. Lett. **55**(5), 633 (2001).
 - [22] T. H. R. Skyrme, Nucl. Phys. **31**, 556 (1962).
 - [23] O. Schwindt, Ph.D. thesis, UMIST (2001).
 - [24] M. Hale, O. Schwindt, and T. Weidig, Phys. Rev. E **62**, 4333 (2000).
 - [25] F. Mandl, *Statistical Physics* (John Wiley, New York, 1988).
 - [26] M. H. Everdell, *Statistical Mechanics and its Chemical Applications* (Academic Press, London, 1975).
 - [27] I. Klebanov, Nucl. Phys. B **262**, 133 (1985).
 - [28] L. Castellejo, P. S. J. Jones, A. S. Jackson, and J. J. M. Verbaarschot, Nucl. Phys. A **501**, 801 (1989).
 - [29] T. S. Walhout, Nucl. Phys. A **484**, 397 (1988).